LASER-MEDIATED SYNTHESIS OF METAL NANOPARTICLES BY OPTICAL VORTEX BEAM

[1,2]Sabrin ABDALLAH, [1,2]Ondřej HAVELKA, [1,2]Jan BRAUN, [1]Rafael TORRES-MENDIETA

[1]Institute for Nanomaterials, Advanced Technologies and Innovation, Technical University of Liberec, Liberec, Czech Republic, EU, sabrin.abdallah@tul.cz, rafael.torres@tul.cz

[2]Faculty of Mechatronics, Informatics and Interdisciplinary Studies, Technical University of Liberec, Liberec, Czech Republic, EU

https://doi.org/10.37904/nanocon.2024.5030

Abstract

Controlling nanoparticles (NPs) morphology in laser-mediated synthesis remains a significant challenge. This study introduces an innovative approach for synthesizing metal NPs using an Optical Vortex Beam (OVB) instead of the conventional Gaussian Beam (GB) in femtosecond laser ablation in liquids (fs-LAL). The primary objective is to achieve NPs shape modification through an environmentally friendly method, eliminating the need for chemical reagents and producing ligand-free NPs suitable for catalytic and biomedical applications. The transformation from GB to OVB was accomplished using a series of waveplates that first converted the linearly polarized GB to a circularly polarized beam and subsequently to a spiral phase wavefront beam, known as OVB. A key innovation of this study is the design of a 3D-printed ablation cell, which generates a thin liquid layer and ensures continuous liquid flow over the metal target, optimizing the laser-ablation setup. This optimization not only enhances productivity but also significantly reduces operation time. Results indicate that using OVB provides superior control over NPs morphology compared to GB, resulting in NPs with improved optical properties, as confirmed by Scanning Transmission Electron Microscopy (STEM) and UV-Vis spectroscopy. This approach holds potential for nanocatalysis, offering a cleaner and more efficient method for NPs synthesis.

Keywords: Laser-mediated synthesis, metal nanoparticles, optical vortex beam, morphology, set-up optimization

1. INTRODUCTION

Laser ablation in liquids (LAL) has emerged as a novel and sustainable method for producing metal nanoparticles (NPs) of high purity. [1] However, a key challenge preventing LAL from reaching its full potential is the precise control of NPs morphology, including size, shape, and surface chemistry. [2, 3] Since the physico-chemical and optical properties of NPs are closely linked to their morphology, fine-tuning these characteristics is essential for optimizing their performance.

Plasmonic NPs (PNPs) like gold (Au) and silver (Ag) are particularly well-studied in this regard due to their unique optical properties, especially the localized surface plasmon resonance (LSPR), which can be enhanced through controlling their shape and structure. [4, 5] This ability to manipulate LSPR makes PNPs highly valuable in applications like sensing, drug delivery, and cancer therapy. [6–9]

As a result, controlling NPs morphology has been extensively studied through various synthetic routes. However, with the growing focus on environmentally friendly practices that align with the principles of green chemistry, LAL has gained significant attention. [10] By using light instead of hazardous chemicals to produce ligand-free NPs, LAL eliminates the need for chemical reagents and stabilizers. This makes laser-generated NPs particularly suitable for applications in fields such as catalysis, photonics, and biomedicine, where ultra-pure NPs are highly desirable. [11]

Although spherical NPs are the most commonly produced in LAL, the versatility of this method- ranging from the choice of target materials and liquid mediums to the modulation of laser parameters such as fluence, wavelength, pulse duration, and beam structure- has led to the exploration of various techniques for shape modification. [1, 12] Techniques such as altering solvents or applying external forces like electric fields, magnetic fields, or heat have been investigated. [13–17] However, these studies, predominantly utilize nanosecond lasers, require lengthy processes (such as suspension aging), result in modest production yield (100–150 mg/L), and generate bi-modal size distributions and/or various structures in a single experiment with some structures exceeding the 100 nm mark. Furthermore, the introduction of surfactants for shape modification contradicts the fundamental objective of LAL, which is to generate pure NPs.

Despite the numerous studies published on this topic, the employment of structurally-modified laser beams remains unexplored. Among the different possibilities for laser beam manipulation, generating an optical vortex beam (OVB) seems the most promising.[18] Due to the helical phase fronts and orbital angular momentum, OVB can capture and set particles into rotation around the beam axis which proved beneficial in various applications like optical tweezers development or quantum entanglement. [19] OVBs have been used for the creation of spiral-like structures on the surface of metals and for trapping and moving particles in liquids and on the surface of materials.[20, 21] In this context, using an OVB instead of a Gaussian Beam (GB) introduces a potentially direct and facile approach for the generation of morphologically modified NPs by LAL.

Moreover, this study considers the importance of the laser ablation setup in ensuring the delivery of a high intensity beam to the target's surface, as well as the experiments' reproducibility. Recent studies indicate that a thin liquid layer on the target's surface can prevent energy loss and enhance productivity up to 15 times compared to the conventional setup. [1, 22] Hence, the design of a 3D printed ablation cell that generates a thin liquid layer and enables a continuous liquid flow over the target's surface is implemented.

In summary, this study aims to compare the effects of GB and OVB on the morphology of Au and titanium (Ti) NPs synthesized by femtosecond LAL (fs-LAL) in a continuous liquid flow setup. By understanding how OVB influences NPs morphology across metals with different ablation thresholds (0.2 J/cm^2 for Au and 0.05 J/cm^2 for Ti) [23, 24], we hope to establish a new methodology for producing shape-controlled NPs that can be tuned for specific applications in catalysis, biomedicine, and beyond.

2. METHODOLOGY

Drawing inspiration from a water wall, the design of an ablation cell for the generation of a thin liquid layer was modeled in Autodesk Fusion 360 software and printed on an i3 MK3S+ 3D printer (Original Prusa) with PETG filament. To generate a continuous liquid flow, a peristaltic pump with 4/6mm silicon tubes operating at 200 ml/min was employed. The ablation cell was attached to two motorized linear stages (8MT193-100, Standa) working at 10 mm/s to ensure consistent ablation along the foil's surface by a 2-axis controller (8SMC5-USB-B9-2, Standa). For the ablation process, a metal foil was placed into the slit of the 3D printed cell as depicted in **Figure 1**, wherein a thin liquid layer was generated by a set of nozzles.

The ablation of an Au or a Ti foil (> 99.99% purity for Au and > 99.7% purity for Ti, Sigma Aldrich) was carried out by a fs-laser (Onefive Origami XP-S, NKT Photonics) operating at 5.1 W, 400 fs, with the wavelength centered at 1030 nm and a repetition rate of 1 MHz. The 3 mm linearly polarized Gaussian Beam (at FWHM) was converted into a circularly polarized GB by a quarter-waveplate (QWP, ThorLabs) placed at 45 °. An S-waveplate (SWP, WOPhotonics) positioned after the QWP converted the circularly polarized GB into an OVB (**Figure 1**). Subsequently, the OVB was expanded by a Galilean telescope (5X) prior to tight focusing with a 25.4 mm plano-convex lens to reach the highest beam intensity on the foil's surface. For experiments employing only GB, the converters were removed from the set-up. The foils were irradiated for 3 h, wherein 40 ml of demiH_2O (18.2 MΩ·cm), and later colloid, was pumped by the peristaltic pumps through a closed-loop system. After irradiation, the colloids were centrifuged for 20 min at 14500 rpm (MiniSpin plus centrifuge,

Eppendorf) to collect the produced NPs in a single 1.5 mL Eppendorf tubes. The samples were stored in a cool and dark place for later characterization.

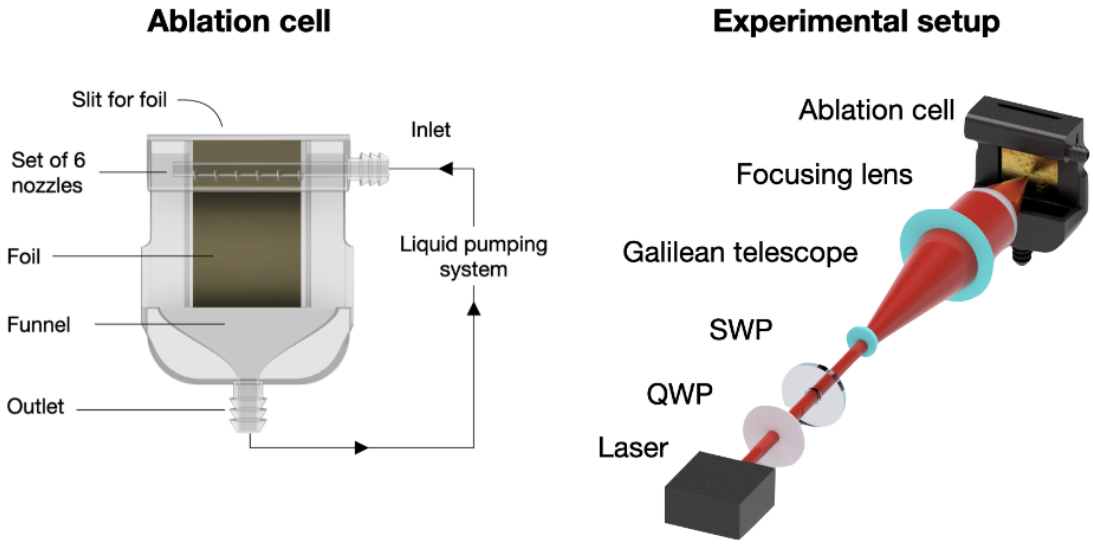

Figure 1: Ablation cell model in Fusion360 with key features explained (left) and the experimental setup for laser ablation of an Au foil with an optical vortex beam (right).

Each sample, labeled based on the type of foil and beam employed, was analyzed by an Ultraviolet–Visible (UV–Vis) spectroscope (Optima 2100Dv, Perkin Elmer) in the range of 220 – 950 nm with a 1 nm resolution to determine the NPs optical properties. Moreover, Scanning Transmission Electron Microscopy (STEM) images were acquired by a focused ion beam microscope (HELIOS 5 PFIM CXe, ThermoFisher Scientific) at 30 kV equipped with a STEM detector to assess the shape and size of the NPs. A drop of the sample was deposited on a formvar/carbon copper grid and dried at room temperature. The size analysis was performed by manually measuring the diameter of 500 NPs.

3. RESULTS AND DISCUSSION

Notably, the visual appearance of the colloids immediately after synthesis revealed significant differences between the samples. The Au-GB colloid exhibited a reddish-purple color, while the Au-OVB colloid displayed a bluish-purple color. Previous studies suggest that Au NPs typically appear red due to their spherical shape, but variations in NPs size and shape can alter the colloid's color. Specifically, Au nanorods, which possess two plasmonic peaks, tend to exhibit a blue coloration, as an additional absorbance peak emerges in the red or near-infrared region. This suggests that the different optical properties observed in our samples could be attributed to variations in NPs morphology.

Thus, based on these observations and the information obtained from the absorbance spectra we can gain an understanding of the shape and size of the NPs, especially in the case of Au NPs. As displayed in **Figure 2**, sample Au-GB has a plasmonic peak centered at 526 nm suggesting the presence of spherical NPs. In contrast, for sample Au-OVB there is a red-shift of the plasmonic peak to 546 nm suggesting the formation of larger spherical NPs or possibly a collective behavior of smaller NPs that are in proximity and acting as a single entity. Moreover, this sample has an additional peak around 633 nm which is an indication of the formation of non-spherical NPs like nanoflowers [25] or nanostars [26], or some degree of agglomeration. However, in both Au spectra a more intense peak is visible at smaller wavelengths (~220 nm). Based on theoretical calculation obtained from the open access Mie calculator from Prof. Lucien Saviot [27] this would suggest the presence of predominantly small NPs, below 10 nm.

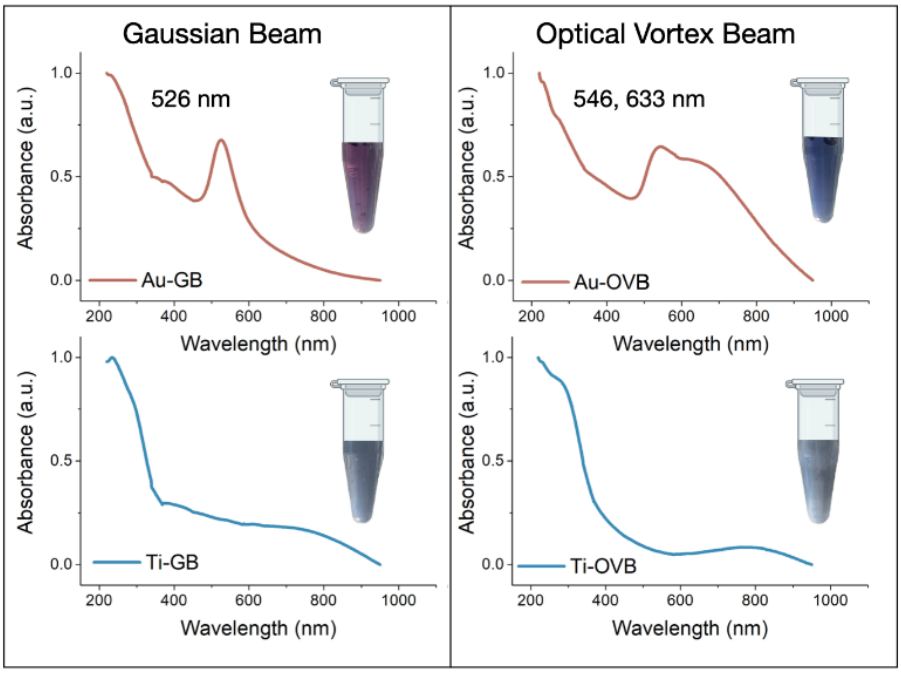

Figure 2 Absorbance spectra of Au and Ti NPs synthesized by a GB and an OVB in the wavelength range of 220 – 950 nm (normalized). The inset images depict the color of each colloid.

In the case of Ti NPs, Ti-GB colloid appeared to have a bluish-grey color, while Ti-OVB colloid appeared grey. In contrast to Au, Ti oxidizes more readily, thus, it is most likely the case that we obtained Ti oxide NPs since the ablation of a Ti foil was carried out in an aqueous environment. Typically, TiO_2 colloid appears white or blue. Sample Ti-GB has an absorbance peak at 230 nm accompanied by a long, broad tail spreading all the way to the near infra-red region which could suggest a wide range of NPs sizes. In the case of Ti-OVB there is an additional peak at 300 nm, which could indicate the presence of larger NPs.

According to the STEM images in **Figure 3**, although both Au-GB and -OVB samples contain spherical NPs, they also contain non-spherical NPs with diameters below 10 nm. This explains the plasmonic behavior observed in the UV region of the spectrum evaluated by the UV-Vis spectroscopy. The Au-GB sample contains predominantly small NPs with a diameter distribution centered at 8.9 nm. Additionally, this sample is characterized by “nanowebs” that create elongated necks linking together NPs. On the other hand, Au-OVB NPs have a smaller diameter centered at 6.9 nm. More importantly, in this case, one can observe elongated NPs that are separated and not forming the nanowebs as in the Au-GB sample. This can be attributed to the fact that the intensity distributions of the GB and OVB are not comparable. GB intensity is distributed in a circle with the highest intensity in the center, in contrast, OVB’s intensity is distributed in a ring. Thus, each beam delivers different energy to the foil’s surface. Even when using the maximum power, we are ablating at a lower fluence with an OVB (excluding the absorption and scattering of the beam along its path by the optical elements). According to Kabashin et al. [28] who performed fs-LAL of Au in water employing various fluences, such small NPs are observed at a lower fluence (<100 J/cm^2). This phenomenon relates to the different mechanisms of NPs formation in LAL as previously explained by Shih et. al. [29] whom, through molecular dynamic calculations could determine that the immediate laser-matter interaction, preceding the ablation process, enables the solid evaporation forming a solid-liquid mixing region which rapidly condensates forming small NPs. In contrast, the larger particles are formed during the nucleation process after ablation. Thus, according to these studies we can infer that the laser intensity reduction excreted by the OVB favors the solid evaporation process, and with it, small NPs formation. However, as Au holds a massive thermal conductivity (318 W/m·K), compared to Ti (11.4 W/m·K), their NPs formation mechanisms may differ.[30] In particular, when experiencing condensation, higher thermal conductivity leads to rapid cooling and with this, the inability to

reach a stable spherical shape, which does not occur with Ti that seems to hold sufficient energy to coalesce until the spheres are formed. When coalescence takes place after the ablation, a high thermal conductivity would be detrimental towards sphere formation, especially when using energies close to the solid targets' ablation threshold, indicating minimal material detachment intervening in the NPs formation leading to metastable shapes as those found in Au that seem to be a middle way to spheres. Moreover, since the OVB carries orbital angular momentum, it can move material immediately after detachment from the solid target. This motion of the detached Au pieces, combined with their high thermal conductivity, appears to influence the coalescence process, and thus, non-spherical particles are formed. In contrast, the GB does not immediately move the detached Au pieces, allowing them to melt and form nanowebs.

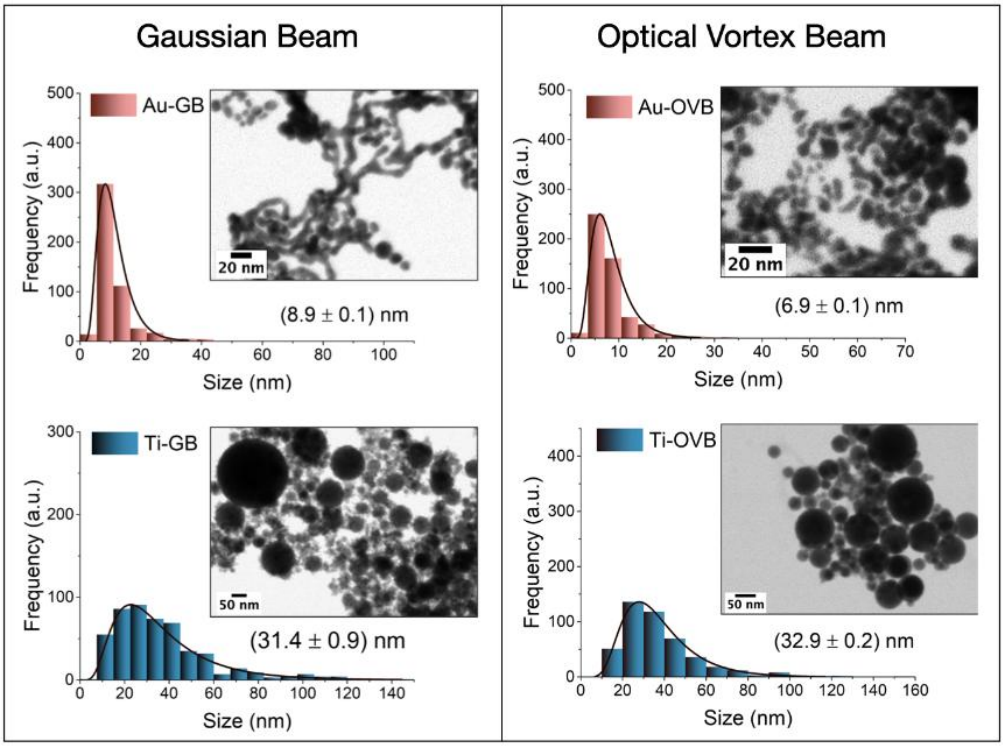

Figure 3 Size distributions of Au and Ti NPs synthesized by a GB and an OVB with log-normal fitting. STEM images of the NPs characteristic of each sample are included.

4. CONCLUSION

In conclusion, this study demonstrates significant differences in the optical and morphological properties of Au and Ti NPs synthesized using GB and OVB in LAL. The Au-OVB sample exhibited a bluish-purple color and a red-shifted plasmonic peak, suggesting the formation of non-spherical NPs, such as nanostars or nanoflowers, while the Au-GB sample displayed a reddish-purple color indicative of spherical NPs. STEM images confirmed these variations in Au-OVB, producing smaller, elongated NPs, however, Au-GB images revealed the formation of nanowebs in addition to larger spherical NPs. These differences are attributed to the unique energy distribution of the OVB, which promotes smaller NPs formation through solid evaporation mechanisms. In the case of Ti, both samples displayed characteristics of Ti oxide, with Ti-GB showing a wider range of NPs sizes and Ti-OVB forming larger particles. The findings highlight the influence of thermal conductivity and beam type on NPs formation, particularly in the case of Au, where high thermal conductivity combined with OVB's orbital angular momentum reduces coalescence and favors non-spherical shapes. While this study enhances understanding of NPs synthesis via LAL, further research is needed to optimize laser parameters and explore how these mechanisms can be applied to other materials.

ACKNOWLEDGEMENTS

The research presented in this article was supported by the Internal Grant of the Technical University of Liberec (SGS-2024-3424).

REFERENCES

[1] ZHANG, Dongshi, Bilal GÖKCE and Stephan BARCIKOWSKI. Laser Synthesis and Processing of Colloids: Fundamentals and Applications. *Chemical Reviews*. 2017, vol. 117, no. 5, pp. 3990–4103. ISSN 0009-2665, 1520-6890.

[2] AMANS, David, Weiping CAI and Stephan BARCIKOWSKI. Status and demand of research to bring laser generation of nanoparticles in liquids to maturity. *Applied Surface Science*. 2019, vol. 488, pp. 445–454. ISSN 01694332.

[3] AMENDOLA, Vincenzo and Moreno MENEGHETTI. What controls the composition and the structure of nanomaterials generated by laser ablation in liquid solution? *Phys. Chem. Chem. Phys*. 2013, vol. 15, no. 9, pp. 3027–3046. ISSN 1463-9076, 1463-9084.

[4] PETRYAYEVA, Eleonora and Ulrich J. KRULL. Localized surface plasmon resonance: Nanostructures, bioassays and biosensing—A review. *Analytica Chimica Acta*. 2011, vol. 706, no. 1, pp. 8–24. ISSN 00032670.

[5] ZHANG, Junxi and Lide ZHANG. Nanostructures for surface plasmons. *Advances in Optics and Photonics*. 2012, vol. 4, no. 2, 157. ISSN 1943-8206.

[6] PLOU, Javier et al. Prospects of Surface-Enhanced Raman Spectroscopy for Biomarker Monitoring toward Precision Medicine. *ACS Photonics*. 2022, vol. 9, no. 2, pp. 333–350. ISSN 2330-4022, 2330-4022.

[7] VERSIANI, Alice F. et al. Gold nanoparticles and their applications in biomedicine. *Future Virology*. 2016, vol. 11. no. 4, pp. 293–309. ISSN 1746-0794, 1746-0808.

[8] BUCHARSKAYA, Alla B. et al. Photothermal and Photodynamic Therapy of Tumors with Plasmonic Nanoparticles: Challenges and Prospects. *Materials*. 2022, vol. 15. no. 4, 1606. ISSN 1996-1944.

[9] TAN, Peng, HeSheng LI, Jian WANG a Subash C.B. GOPINATH. Silver nanoparticle in biosensor and bioimaging: Clinical perspectives. *Biotechnology and Applied Biochemistry*. 2020, vol. 68, no. 6, pp. 1236–1242. ISSN 0885-4513, 1470-8744.

[10] HAVELKA, Ondřej et al. On the Use of Laser Fragmentation for the Synthesis of Ligand-Free Ultra-Small Iron Nanoparticles in Various Liquid Environments. *Nanomaterials*. 2021, vol. 11, no. 6, 1538. ISSN 2079-4991.

[11] ETTEL, David et al. Laser-synthesized Ag/TiO nanoparticles to integrate catalytic pollutant degradation and antifouling enhancement in nanofibrous membranes for oil–water separation. *Applied Surface Science*. 2021, vol. 564, 150471. ISSN 01694332.

[12] SUBHAN, Abdul, Abdel-Hamid Ismail MOURAD and Yarub AL-DOURI. Influence of Laser Process Parameters, Liquid Medium, and External Field on the Synthesis of Colloidal Metal Nanoparticles Using Pulsed Laser Ablation in Liquid: A Review. *Nanomaterials*. 2022, vol. 12, no. 13, 2144. ISSN 2079-4991.

[13] BESNER, Sébastien, Andrei V. KABASHIN, Françoise M. WINNIK and Michel MEUNIER. Synthesis of Size-Tunable Polymer-Protected Gold Nanoparticles by Femtosecond Laser-Based Ablation and Seed Growth. *The Journal of Physical Chemistry C*. 2009, vol. 113, no. 22, pp. 9526–9531. ISSN 1932-7447, 1932-7455.

[14] FRIAS BATISTA, Laysa M. et al. Kinetic Control of $[AuCl_4]^-$ Photochemical Reduction and Gold Nanoparticle Size with Hydroxyl Radical Scavengers. *The Journal of Physical Chemistry B*. 2019, vol. 123, no. 33, pp. 7204–7213. ISSN 1520-6106, 1520-5207.

[15] LIN, X. Z. et al. Synthesis of CuO Nanocrystals and Sequential Assembly of Nanostructures with Shape-Dependent Optical Absorption upon Laser Ablation in Liquid. *The Journal of Physical Chemistry C*. 2009, vol. 113, no. 40, pp. 17543–17547. ISSN 1932-7447, 1932-7455.

[16] TSUJI, Takeshi et al. Morphological changes from spherical silver nanoparticles to cubes after laser irradiation in acetone–water solutions via spontaneous atom transportation process. *Colloids and Surfaces A: Physicochemical and Engineering Aspects*. 2017, vol. 529, pp. 33–37. ISSN 09277757.

[17] PIOTTO, Valentina, Lucio LITTI and Moreno MENEGHETTI. Synthesis and Shape Manipulation of Anisotropic Gold Nanoparticles by Laser Ablation in Solution. *The Journal of Physical Chemistry C*. 2020, vol. 124, no. 8, pp. 4820–4826. ISSN 1932-7447, 1932-7455.

[18] RUBINSZTEIN-DUNLOP, Halina et al. Roadmap on structured light. *Journal of Optics*. 2017, vol. 19, no. 1, 013001. ISSN 2040-8978, 2040-8986.

[19] SHEN, Yijie et al. Optical vortices 30 years on: OAM manipulation from topological charge to multiple singularities. *Light: Science & Applications* [online]. 2019, vol. 8, no. 1, 90. ISSN 2047-7538. Available from: doi:10.1038/s41377-019-0194-2

[20] LEHMUSKERO, Anni et al. Laser Trapping of Colloidal Metal Nanoparticles. *ACS Nano*. 2015, vol. 9, no. 4, pp. 3453–3469. ISSN 1936-0851, 1936-086X.

[21] TOYODA, Kohei et al. Using Optical Vortex To Control the Chirality of Twisted Metal Nanostructures. *Nano Letters*. 2012, vol. 12, no. 7, pp. 3645–3649. ISSN 1530-6984, 1530-6992.

[22] MESSINA, Gabriele C. et al. Pulsed laser ablation of a continuously-fed wire in liquid flow for high-yield production of silver nanoparticles. *Phys. Chem. Chem. Phys.* 2013, vol. 15, no. 9, pp. 3093–3098. ISSN 1463-9076, 1463-9084.

[23] KRÜGER, Jörg, Daniela DUFFT, Robert KOTER and Andreas HERTWIG. Femtosecond laser-induced damage of gold films. *Applied Surface Science*. 2007, vol. 253, no. 19, pp. 7815–7819. ISSN 01694332.

[24] WANG, Liming et al. Surface chemistry of gold nanorods: origin of cell membrane damage and cytotoxicity. *Nanoscale*. 2013, vol. 5, no. 18, 8384. ISSN 2040-3364, 2040-3372.

[25] WOŹNIAK, Anna et al. Size and shape-dependent cytotoxicity profile of gold nanoparticles for biomedical applications. *Journal of Materials Science: Materials in Medicine*. 2017, vol. 28, no. 6, 92. ISSN 0957-4530, 1573-4838.

[26] MINATI, Luca, Filippo BENETTI, Andrea CHIAPPINI and Giorgio SPERANZA. One-step synthesis of star-shaped gold nanoparticles. *Colloids and Surfaces A: Physicochemical and Engineering Aspects*. 2014, vol. 441, pp. 623–628. ISSN 09277757.

[27] SAVIOT, Lucien. Mie scattering calculator. *French National Centre for Scientific Research*. [viewed 2024-01-10]. Available from: https://saviot.cnrs.fr/mie/index.en.html

[28] KABASHIN, A. V. and M. MEUNIER. Synthesis of colloidal nanoparticles during femtosecond laser ablation of gold in water. *Journal of Applied Physics*. 2003, vol. 94, no. 12, pp. 7941–7943. ISSN 0021-8979, 1089-7550.

[29] SHIH, Cheng-Yu et al. Two mechanisms of nanoparticle generation in picosecond laser ablation in liquids: the origin of the bimodal size distribution. *Nanoscale*. 2018, vol. 10, no. 15, pp, 6900–6910. ISSN 2040-3364, 2040-3372.

[30] TOULOUKIAN, Y S, R W POWELL, C Y HO and P G KLEMENS. *Thermophysical properties of matter - the TPRC data series. Volume 1. Thermal conductivity - metallic elements and alloys. (Reannouncement). Data book*. 1970.